◆ ISES ENDOVASCULAR RESEARCH COMPETITION, FIRST PLACE ◆

Computational Analysis of Stresses Acting on Intermodular Junctions in Thoracic Aortic Endografts

Anamika Prasad, PhD[1]; Lillian K. To, MSc[2]; Madhu L. Gorrepati, MD[3]; Christopher K. Zarins, MD[3]; and C. Alberto Figueroa, PhD[1]

Departments of [1]Bioengineering, [2]Biology, and [3]Surgery, Stanford University, Stanford, California, USA.

Purpose: To evaluate the biomechanical and hemodynamic forces acting on the intermodular junctions of a multi-component thoracic endograft and elucidate their influence on the development of type III endoleak due to disconnection of stent-graft segments.

Methods: Three-dimensional computer models of the thoracic aorta and a 4-component thoracic endograft were constructed using postoperative (baseline) and follow-up computed tomography (CT) data from a 69-year-old patient who developed type III endoleak 4 years after stent-graft placement. Computational fluid dynamics (CFD) techniques were used to quantitate the displacement forces acting on the device. The contact stresses between the different modules of the graft were then quantified using computational solid mechanics (CSM) techniques. Lastly, the intermodular junction frictional stability was evaluated using a Coulomb model.

Results: The CFD analysis revealed that curvature and length are key determinants of the displacement forces experienced by each endograft and that the first 2 modules were exposed to displacement forces acting in opposite directions in both the lateral and longitudinal axes. The CSM analysis revealed that the highest concentration of stresses occurred at the junction between the first and second modules of the device. Furthermore, the frictional analysis demonstrated that most of the surface area (53%) of this junction had unstable contact. The predicted critical zone of intermodular stress concentration and frictional instability matched the location of the type III endoleak observed in the 4-year follow-up CT image.

Conclusion: The region of larger intermodular stresses and highest frictional instability correlated with the zone where a type III endoleak developed 4 years after thoracic stent-graft placement. Computational techniques can be helpful in evaluating the risk of endograft migration and potential for modular disconnection and may be useful in improving device placement strategies and endograft design.

J Endovasc Ther. 2011;18:559–568

Key words: stent-graft, thoracic aortic endografts, migration, component disconnection, displacement forces, contact stresses, frictional stability, intermodular disjunction, thoracic aortic aneurysm, computational solid mechanics, computational fluid dynamics

This study was supported by the National Institutes of Health grant 1 RC EB011443. In accordance with the NIH Public Access Policy, this article is available for open access at PubMed Central.

The authors have no commercial, proprietary, or financial interest in any products or companies described in this article.

Address for correspondence and reprints: C. Alberto Figueroa, PhD, Department of Bioengineering, Clark Center E382, 318 Campus Drive West, Stanford, CA 94305-5431 USA. E-mail: *cafa@stanford.edu*

Thoracic endovascular aortic repair (TEVAR) has developed rapidly in the last 15 years; today, tens of thousands of procedures are performed yearly in the United States alone.[1,2] Initially used primarily in older patients who could not tolerate invasive open repair, TEVAR is now applied to treat a broad range of patients and aneurysm morphologies. Although the short-term outcomes of TEVAR have been favorable compared to open repair, the long-term outcomes often present complications, such as aneurysm enlargement, endograft collapse, endoleaks, and device migration.[3–5] Consequently, TEVAR patients often require costly periodic screenings to assess the positional and structural stability of the device and the state of the aneurysm.

Type III endoleaks result from disconnection of the different modules used in the stent-graft to bridge the length of the aneurysm.[6] Indeed, several endograft modules are usually deployed longitudinally with various degrees of oversizing and overlapping among the device components. These devices are exposed to the unique biomechanical environment of the thoracic aorta, where significant aortic wall motion and highly pulsatile flow and pressure conditions pose significant challenges to the structural integrity of the device modules and their junctions. A deeper understanding of the forces experienced by endografts in vivo and of the frictional response developed at intermodular junctions may help to improve the performance and long-term durability of thoracic stent-grafts. While previous studies have investigated the patient-specific 3-dimensional (3D) actions of blood flow on thoracic aortic endografts,[7] no study thus far has analyzed the contact stresses developed at the intermodular junctions of the different stent-graft modules utilized in TEVAR.

We have developed a method using computational solid mechanics (CSM) and computational fluid dynamics (CFD) techniques to quantitate the in vivo displacement force acting on each endograft module, as well as the intermodular contact stress and frictional response using patient-specific contrast-enhanced computed tomography (CT) scans as a basis for analysis. In this study, we applied this method to a patient who required 4 endograft modules to treat a long and tortuous aneurysm in the descending thoracic aorta. The endograft migrated over time, and after 4 years, a type III endoleak developed due to disjunction of the first and second segments of the endograft. The purpose of this report is to present the results of our computational analysis of this stent-graft scenario in relation to the clinical course and long-term in vivo device performance.

METHOD

Patient Data

Anonymized postoperative (baseline) and follow-up CT angiography data (512×512×270 voxels, in-plane resolution of 0.78×0.78 mm, slice thickness 1.25 mm) from a 69-year-old woman (167 cm tall weighing 74 kg) who underwent thoracic aortic aneurysm (TAA) repair with a 4-module thoracic stent-graft (measurements given in Table 1) were used in this study. The postoperative length and diameter of the aneurysm were 125 and

TABLE 1
Dimensions of the 4 Modules Used for TAA Repair, the Nominal Diameter Used in the CSM Analysis, and the Length of the Intermodular Junctions in the Postoperative Configuration

	Module 1	Module 2	Module 3	Module 4
Size, mm*	44 × 120 × 38	42 × 120 × 40	44 × 90 × 46	46 × 111 × 46
Nominal diameter, mm	38	40	44	44
	Modules 1 and 2	Modules 2 and 3	Modules 3 and 4	
Length, mm	21	41	72	

* Proximal diameter × length × distal diameter.

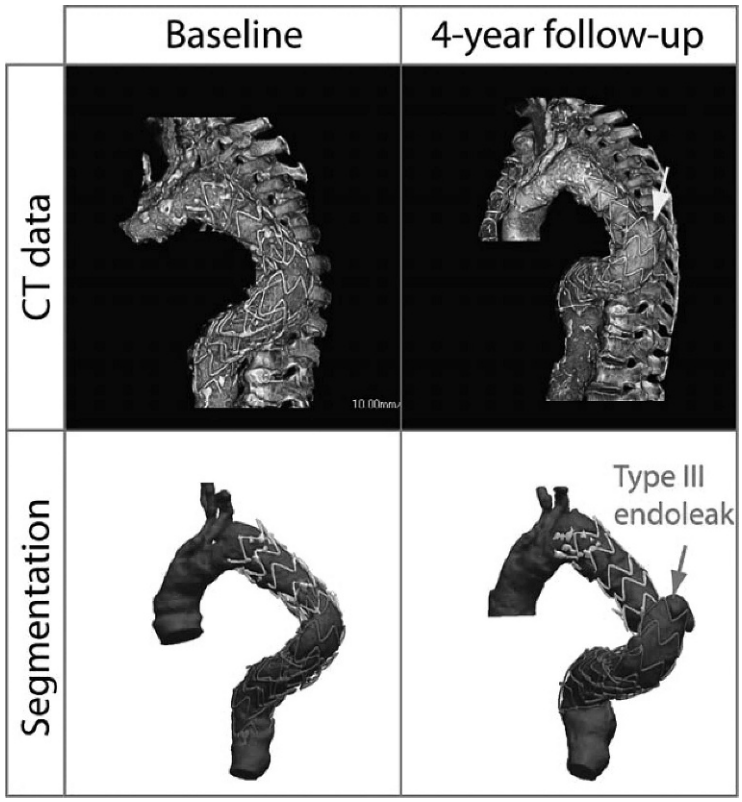

Figure 1 ◆ Computed tomography data (above) and computer segmentations of the thoracic aorta and stents (below) in the baseline (left) and 4-year follow-up configurations (right). Note the type III endoleak in the follow-up images at the intermodular disjunction of the first and second stent-grafts.

69 mm, respectively; the patient's systolic/diastolic/mean blood pressure was 128/59/82 mmHg postoperatively (heart rate 78 bpm and 4.9-L/min cardiac output). Four years after TEVAR, a type III endoleak (Fig. 1) was observed adjacent to a disconnection of the first and second stent-graft components. The endoleak led to a significant increase in aneurysm size (from 69 to 83 mm); the tortuosity and length of the aneurysm also increased significantly. The type III endoleak was repaired using 2 additional endografts deployed using a body floss technique via a brachial exposure.

Model Design

Using this CT data, a patient-specific 3D computer model of the TAA was created using open-source image segmentation software[8] and in-house mesh generation routines.[9] The model included data from the ascending thoracic aorta, aortic arch, descending thoracic aorta, brachiocephalic trunk, left common carotid artery, left subclavian artery, and the stents of the different modules of the device (Fig. 2). A model of the 4-module endograft was constructed in the Abaqus FEA software (Dassault Systèmes Simulia Corporation, Providence, RI, USA). A CFD analysis was performed to simulate blood flow and pressure in the endograft using techniques developed in-house that enabled accurate representation of the TAA geometry and of the postoperative hemodynamic variables (i.e., cardiac output, heart rate, and systolic and diastolic blood pressure).[8–13] Once the CFD analysis was completed, the magnitude and direction of the time-varying displacement forces (DF) acting on each of the 4 modules (i.e., DF_1, DF_2, DF_3, DF_4; see Fig. 2) of the endograft were calculated.

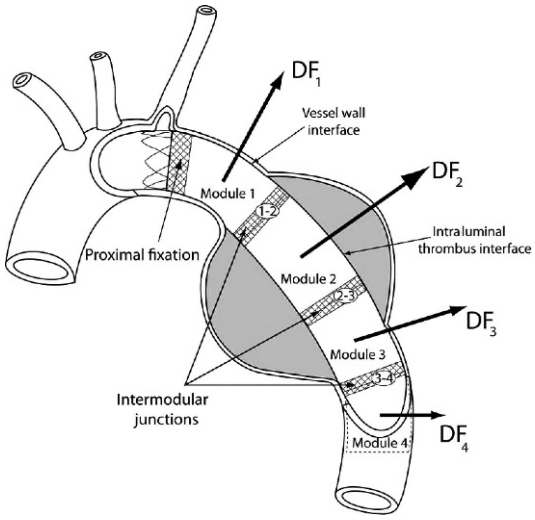

Figure 2 ◆ Schematic of the methodology proposed to study intermodular junction stability of thoracic stent-grafts. Here, 4 modules are subjected to displacement forces (DF) obtained via CFD analysis. These 4 modules define 3 intermodular junctions susceptible to endograft slippage that may lead to type III endoleaks over time. The endografts are constrained externally by either the vessel wall or the intraluminal thrombus interfaces. Contact mechanics formulations were used to deploy the 4 modules of the endograft, then the frictional stability at each of the 3 intermodular junctions was investigated using a Coulomb frictional model implemented in the Abaqus FEA software.[15]

A CSM analysis was then performed whereby 4 stent-grafts were deployed along the centerline axis of the thoracic aorta model using the same dimensions (i.e., diameter and length), overlap lengths, and relative oversizing as those utilized in the actual endovascular repair. Once these 4 modules were deployed and contact was established at each intermodular junction, the endografts were subjected to the displacement forces obtained in the CFD analysis to investigate the concentration of stresses and frictional response at each junction.[14,15] Finally, the percentage of each intermodular junction having unstable contact was evaluated using a Coulomb frictional model,[15,16] and the ''degree of slippage'' of the junctions was correlated with the type III endoleak arising between the first and second segments of the endograft.

CFD Analysis

The endograft computer model representing the postoperative configuration depicted in Figure 2 was discretized into a finite element mesh consisting of 1.7×10^6 linear tetrahedrons and 440,000 nodes. A CFD analysis was run to simulate blood flow and blood pressure for several cardiac cycles until the solution became periodic in time (1-millisecond time increment); in this analysis, both the thoracic aorta and the endograft were assumed to behave in a rigid manner. The magnitude and direction of the time-varying displacement forces [expressed in Newtons (N)] exerted by the blood flow on the different endograft modules were calculated by integrating the distribution of tractions (pressure and the shearing stresses of blood) acting on the surface of the devices.

CSM Analysis

For the purposes of this analysis, the diameter of each module (see Table 1) was considered constant through the length of the device.

Endograft equivalent radial stiffness. Because this work examined the contact stresses resulting from the radial forces developed at the intermodular junctions, the radial stiffness as a function of device oversizing was a critical component of the analysis. It was reasonable to assume that the graft had little contribution to the overall radial stiffness of the device. Therefore, in order to reduce the computational expense of this analysis while still characterizing the radial force response of the stent-grafts correctly, each stent-graft module was modeled as a homogeneous graft whose radial stiffness was chosen to match the radial stiffness of a nitinol[17] Z stent (Fig. 3) subjected to a radial strain of up to 10%. The radial stiffness of the homogenized stent-graft module was set to $K_{Graft} = 1.3$ N. The 4 homogenized modules where discretized into a finite element mesh of 25,500 triangular shell elements and 13,000 nodes.

Endograft fitting. Once the equivalent radial stiffness of the 4 endografts was obtained, the endograft modules were fitted along the centerline path of the patient's thoracic aorta to activate the contact between the different

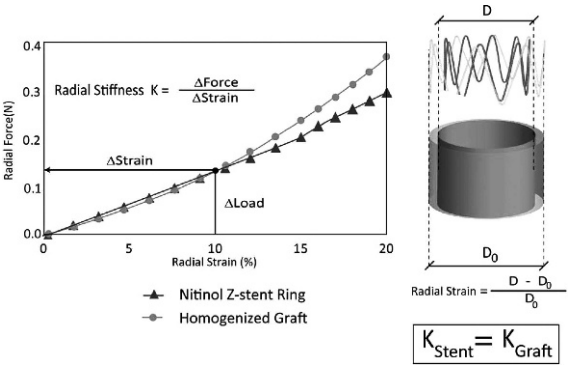

Figure 3 ◆ Stress-strain curves of a nitinol Z stent and the homogenized graft adopted in this study. The radial stiffness of the homogenized graft was determined by matching the radial stiffness of the Z stent over a range of radial strains up to 10%. The equivalent endograft radial stiffness was set to $K_{Graft} = 1.3$ N. This approach significantly simplifies the computational expense of the CSM contact and friction calculations while still correctly representing the radial force response of the stent-graft.

device modules. This contact was characterized by the radial forces developed by each device, by the CFD displacement forces, and by the frictional characteristics between devices at the junctions. In the schematic representation of the steps performed to fit the various endograft modules, Figure 4A depicts a junction where the proximal module (1) is generally of smaller diameter than the distal module (2). The distal part of the proximal module is expanded using a pressure P_{gf} to accommodate the larger distal module (Fig. 4B). Next, the pressure P_{gf} is released, and the intermodular contact is established at the junction (Fig. 4C). The constraining effect of the surrounding tissue (i.e., aortic wall and intraluminal thrombus) through the length of the endograft was modeled via a uniform pressure (P_A) of 20 mmHg acting on the outer surfaces of the endograft modules (Fig. 4D). A 5% radial compression was applied at the endograft junctions to account for the endograft oversizing relative to the nominal diameter of the aorta (Fig. 4E). Lastly, the CFD displacement forces were applied to each module, assuming uniform distribution of each displacement force through the surface of each endograft (Fig. 4F).

Endograft junction frictional analysis. The contact between 2 devices at each intermodular junction was defined by a contact pressure (P_c)

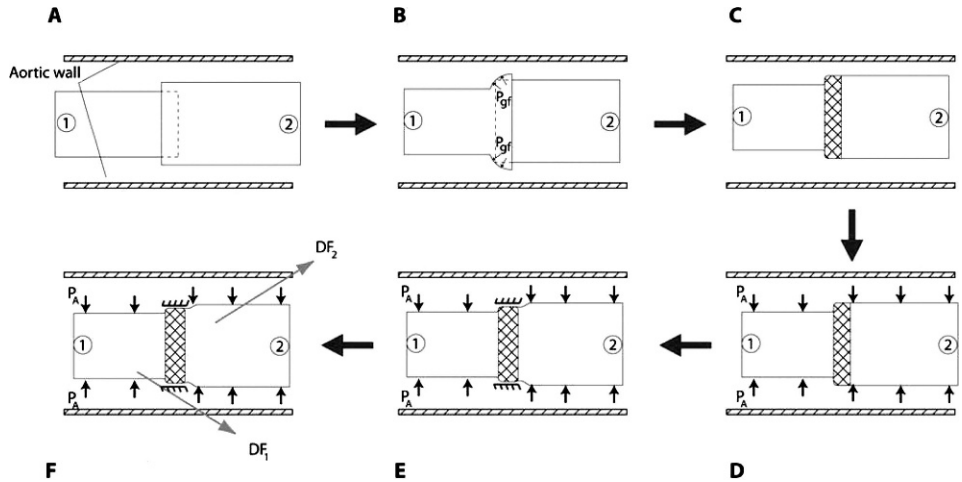

Figure 4 ◆ Schematic representation of the steps performed during the process of endograft fitting: (**A**) configuration of a typical junction where the diameter of the proximal module is smaller than that of the distal module; (**B**) the distal part of the proximal module is expanded to accommodate the larger diameter of the distal module; (**C**) contact is established at the intermodular junction; (**D**) the constraining effect of the external tissue is modeled via a uniform external pressure (P_A); (**E**) a 5% radial compression is applied at the endograft junctions; and (**F**) the CFD displacement forces are applied to each of the deployed endograft modules.

TABLE 2
Components of the Displacement Forces (DF) Acting on Each Endograft Module in the Anterior, Lateral, and Longitudinal Directions, as Well as Magnitude of the Total DF Vector

	Fx (Anterior)	Fy (Lateral)	Fz (Longitudinal)	Total, N
DF_1	−6.7 (−9.5, −4.2)	−4.9 (−7.0, −3.0)	−0.3 (−0.4, −0.2)	8.3 (5.2, 11.8)
DF_2	−12.6 (−18.1, −7.9)	4.6 (2.9, 6.6)	1.0 (0.7, 1.5)	13.4 (8.4, 19.3)
DF_3	−0.2 (−0.2, −0.1)	2.6 (1.6, 3.7)	−4.0 (−5.7, −2.5)	4.7 (2.9, 6.8)
DF_4	3.2 (2.0, 4.7)	−5.8 (−8.5, −3.6)	6.7 (4.2, 9.8)	9.4 (5.9, 13.8)

Data are presented as the time-average of the DF over the cardiac cycle as well as the range between systole and diastole in parentheses.

that acted perpendicular to the surface of the junction and a contact shear (τ_c) that acted tangentially to the surface of the junction. To study the frictional stability of the intermodular connections, a Coulomb model was used with the following stability and slippage conditions[16]:

$$\text{Stable contact} : \tau_c < \mu \cdot P_c$$

$$\text{Unstable contact (slippage)} : \tau_c \geq \mu \cdot P_c,$$

where μ represents the friction coefficient between the surfaces (e.g., the stent and graft material). The actual numerical value of this coefficient must be determined experimentally; based on published data for frictional coefficients between the aortic wall and stent-grafts,[18] a μ of 0.75 was chosen, assuming that the degree of roughness between 2 stent-grafts was higher than that between the wall and the stent-graft. The "slippage coefficient" was defined as the ratio τ_c / $\mu \cdot P_c$. Therefore, a slippage coefficient ≥ 1 indicated unstable contact. In this study, the slippage coefficient was calculated through the surface of each of the intermodular junctions.

RESULTS

CFD Analysis

After completing the CFD simulation of flow and pressure in the postoperative endograft configuration, the displacement forces acting on each of the modules of the device were extracted. Table 2 provides the components of the DF vector in the anterior, lateral, and longitudinal directions, as well as the total magnitude of the displacement forces acting on each stent-graft. Each cell contains the time-average of the displacement forces over the cardiac cycle, together with the diastolic and systolic values.

Figure 5 depicts the forces acting on each stent-graft in the anterior and lateral views. The second module is exposed to the largest displacement force (13.4 N), acting primarily in the anteroposterior direction. Conversely, the third module is subjected to the smallest DF (4.7 N), acting primarily in the lateral (right-to-left) direction. The third device is the shortest of the modules (90 mm), whereas the second module is, together with the first module, the longest (120 mm). These findings are consistent with previous studies that showed that the magnitude of the DF vector is related to the length of the stent-graft: the larger the device, the larger the force.[7,19] In general, the orientation of the DF follows the main curvature of each endograft module. Indeed, this can be observed in the lateral view, where the displacement forces of modules 1, 2, and 3 act in the anteroposterior direction, whereas the displacement force of module 4 points in the posteroanterior direction, following the change in curvature of the device. Figueroa et al.[20] reported similar findings relating to the orientation of the displacement forces with the curvature of the endograft.

Lastly, it is interesting to note that the displacement forces of modules 1 and 2 act in opposite directions in both the lateral (−4.9 N vs. 4.6 N) and longitudinal directions (−0.3 N vs. 1.0 N). These opposing displacement forces may result in a higher concentration of stresses at the first intermodular junction.

CSM Analysis

Intermodular stresses. Figure 6A shows the increment in von Mises stresses experienced

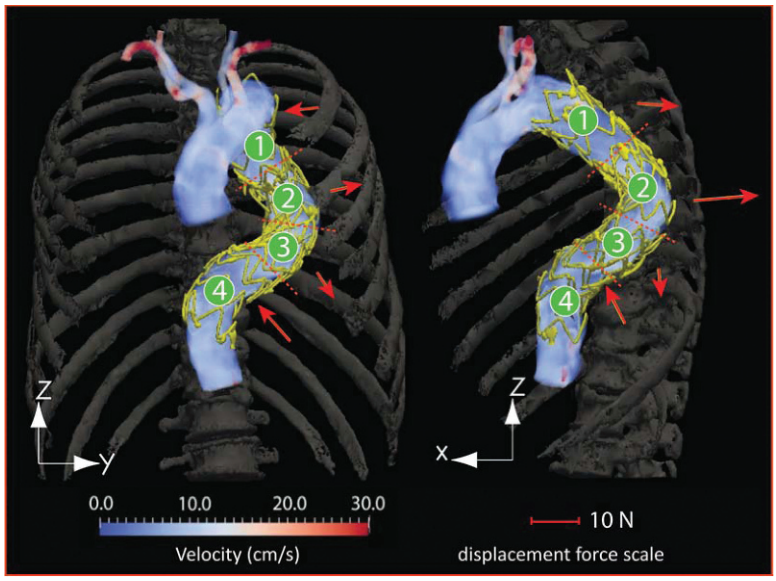

Figure 5 ◆ CFD results showing the mean DF vector (arrows) acting on the different endograft modules 1–4 in the anterior (left) and lateral (right) views.

by the endograft modules due to the action of the displacement forces (i.e., the increment in stress the endografts experience between steps E and F depicted in Figure 4). These stresses at the various endograft junctions result from the combined action of the radial and displacement forces of blood flow. The figure indicates that the maximum concentration of stresses occurs at the junction between modules 1 and 2 (maximum stress of 1.30 MPa). The maximum stresses at the other junctions are significantly smaller: 0.3 and 0.4 MPa on junctions 2–3 and 3–4, respectively. The higher concentration of stresses in junction 1–2 can be explained by factors such as the high curvature of the junction, the opposing DF acting on the proximal and distal modules, and the relatively short overlapping length between modules 1 and 2. These findings correlate with the observed clinical outcome of the device, given by the intermodular separation at this location over the course of a 4-year follow-up, resulting in a type III endoleak.

Endograft junction frictional analysis. Figure 6B shows that junction 1–2 has most of its surface area (53%) in a slipping, unstable state. The area under slippage is significantly smaller in junctions 2–3 (33%) and 3–4 (18%). Furthermore, junctions 2–3 and 3–4 overlap with each other, making it difficult for an endoleak to develop in that region due to the 3-module overlap. These findings are once again consistent with the observed clinical outcome.

DISCUSSION

Endografts used in TEVAR are designed to exclude flow from the aneurysm sac by fixation and seal to the nonaneurysmal thoracic aorta proximal and distal to the aneurysm. Sometimes, this span can be covered with a single endograft module. However, more often than not, several endograft modules are required to treat the full extent of the thoracic aneurysm. The overlapped junctions between these modules can shift over time, resulting in dislocation and complete disconnection of the endograft components, giving rise to a type III endoleak. Thus, a deeper understanding of the forces experienced by endografts in vivo and of the frictional response developed at intermodular junctions is required in order to improve the performance and long-term durability of thoracic stent-grafts.

Using CFD techniques we developed to evaluate the displacement forces acting on thoracic aortic endografts based on patient-specific anatomical data from postoperative

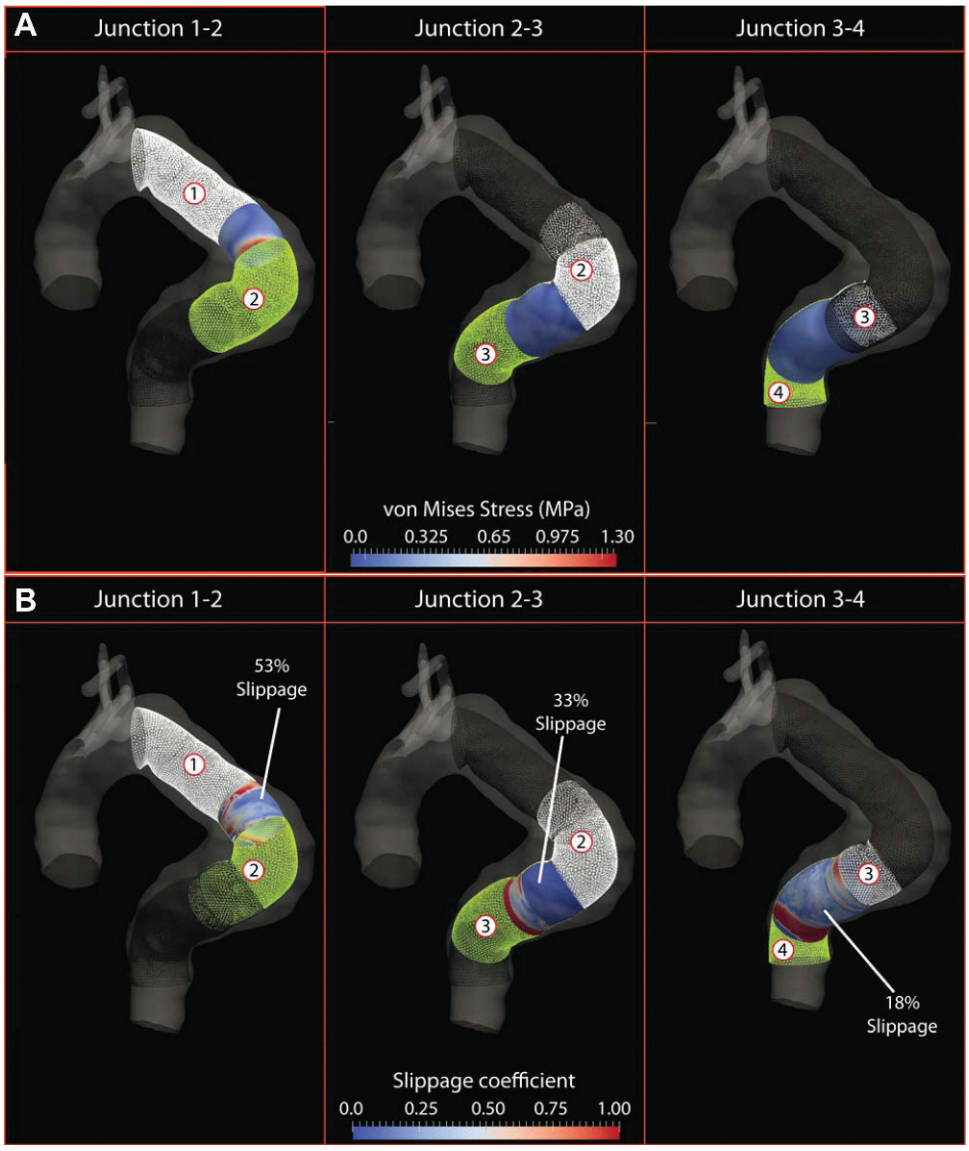

Figure 6 ◆ (**A**) Intermodular stress analysis shows that the highest concentration of stress increments occurs at junction 1–2, the site of development of the type III endoleak. (**B**) Endograft frictional stability analysis shows that junction 1–2 has most of its surface area (53%) under slipping conditions. The slippage areas in the other 2 junctions are significantly smaller (33% and 18%, respectively).

CTA scans,[7,20] we showed that the magnitude and direction of these forces are determined by factors such as endograft length and diameter, aortic curvature, and blood pressure. In this study, we examined the radial forces and frictional characteristics that ultimately define the stability of a multi-component thoracic endograft.

Based on CT data from a long, tortuous 125-mm descending TAA that eventually developed a type III endoleak due to modular disconnection, we found that the longer the device and the larger the curvature, the larger the displacement forces acting on the stent-graft. Moreover, the first 2 modules were exposed to displacement forces that acted in opposite directions in both the lateral and longitudinal axes. These opposing displacement forces resulted in a high concentration of stresses at the first intermodular junction.

In this particular patient, the relatively short length (21 mm) of the junction and this concentration of stresses contributed to the intermodular separation that took place over the course of a 4-year follow-up. This observation was further supported by the frictional stability analysis, which revealed that junction 1–2 had most of its surface area (53%) in a slipping, unstable state.

Limitations

The analysis presented here is just a first step toward assessing the structural stability of thoracic endografts in vivo. In the CFD analysis, we did not consider the effect of the compliance of the aortic wall or the endograft. In the CSM analysis, we modeled the radial strength of each module using a simple homogenized graft material of equivalent radial stiffness, thus overestimating the bending stiffness of each of the endograft modules. Furthermore, since the study was concerned with endograft intermodular stability, we did not model the interactions between the proximal and distal fixation zones of the device and the aortic wall, assuming that the endograft was fixed at both locations. Our analysis represented the effect of external tissues (i.e., aortic wall and intramural thrombus) using a uniform pressure acting on the outer surface of the endografts. However, the effects of external tissue are much more complex in real life. Future work will include appropriate constitutive models for the different tissues in order to explicitly represent their interactions with the device. Lastly, our CSM analysis considered only the temporal mean of the displacement force uniformly distributed through the surface of the endograft. In reality, the displacement forces vary spatially and temporally, and these variations may play an important role in the evolution of contact stresses at the endograft junctions.

Conclusion

We have developed a new computational modeling technique to quantitatively assess in vivo biomechanical forces acting on thoracic aortic endografts and their intermodular components, with clinical correlation to modular disconnection data provided by a longitudinal imaging study. These techniques combined advances in medical image segmentation, computational fluid dynamics, and computational solid mechanics to provide unique insight into the complex contact interactions between the different modules usually utilized in a TEVAR procedure. The techniques may improve our ability to identify endograft failure modes and may ultimately assist in future endograft designs and treatment planning. Future studies will determine whether these techniques can predict the risk of device failure in individual patients.

REFERENCES

1. Dake MD, Miller DC, Semba CP, et al. Transluminal placement of endovascular stent-grafts for the treatment of descending thoracic aortic aneurysms. *N Engl J Med*. 1994;331:1729–1734.
2. Dake MD, Miller DC, Mitchell RS, et al. The ''first generation'' of endovascular stent-grafts for patients with aneurysms of the descending thoracic aorta. *J Thorac Cardiovasc Surg*. 1998; 116:689–704.
3. Leurs LJ, Bell R, Degrieck Y, et al. Endovascular treatment of thoracic aortic diseases: combined experience from the EUROSTAR and United Kingdom Thoracic Endograft registries. *J Vasc Surg*. 2004;40:670–680.
4. Bavaria JE, Appoo JJ, Makaroun MS, et al. Endovascular stent grafting versus open surgical repair of descending thoracic aortic aneurysms in low-risk patients: a multicenter comparative trial. *J Thorac Cardiovasc Surg*. 2007;133:369–377.
5. Matsumura JS, Cambria RP, Dake MD, et al. International controlled clinical trial of thoracic endovascular aneurysm repair with the Zenith TX2 endovascular graft: 1-year results. *J Vasc Surg*. 2008;47:247–257.
6. Hansen CJ, Bui H, Donayre CE, et al. Complications of endovascular repair of high-risk and emergent descending thoracic aortic aneurysms and dissections *J Vasc Surg*. 2004;40:228–234.
7. Figueroa CA, Taylor CA, Chiou AJ, et al. Magnitude and direction of pulsatile displacement forces acting on thoracic aortic endografts. *J Endovasc Ther*. 2009;16:350–358.
8. Yushkevich PA, Piven J, Hazlett HC, et al. User-guided 3D active contour segmentation of anatomical structures: significantly improved efficiency and reliability. *Neuroimage*. 2006;31: 1116–1128.

9. Xiong G, Figueroa CA, Xiao N, et al. Simulation of blood flow in deformable vessels using subject-specific geometry and spatially varying wall properties. *Int J Numer Meth Biomed Engin*. 2010 Jul 20, DOI: 10.1002/cnm.1404
10. Vignon-Clementel IE, Figueroa CA, Jansen KE, et al. Outflow boundary conditions for three-dimensional finite element modeling of blood flow and pressure in arteries. *Comput Meth Appl Mech Eng*. 2006;195:3776–3796.
11. Kim HJ, Vignon-Clementel IE, Figueroa CA, et al. On coupling a lumped parameter heart model and a three-dimensional finite element aorta model. *Ann Biomed Eng*. 2009;37: 2153–2169.
12. Sahni O. Efficient anisotropic adaptive discretization of the cardiovascular system. *Comput Methods Biomech Biomed Engin*. 2006;195:5634–5655.
13. Taylor CA, Figueroa CA. Patient-specific modeling of cardiovascular mechanics. *Ann Rev Biomed Eng*. 2009;11:109–134.
14. Johnson K. *Contact Mechanics*. Cambridge, UK: Cambridge University Press; 1987.
15. Simulia: Abaqus Theory Manual, version 6.8; available at: *http://www.simulia.com/support/documentation.html*
16. Hutchings IM. *Tribology: Friction and Wear of Engineering Materials*. London, UK: Elsevier Limited; 1992.
17. Kleinstreuer C, Li Z, Basciano CA, et al. Computational mechanics of nitinol stent grafts. *J Biomech*. 2008;41:2370–2378.
18. Vad S, Eskinazi A, Corbett T, et al. Determination of coefficient of friction for self-expanding stent-grafts. *J Biomech Eng*. 2010;132:121007.
19. Li Z, Kleinstreuer C, Farber M. Computational analysis of biomechanical contributors to possible endovascular graft failure. *Biomech Model Mechanobiol*. 2005;4:221–234.
20. Figueroa CA, Taylor CA, Yeh V, et al. Effect of curvature on displacement forces acting on aortic endografts: a 3-dimensional computational analysis. *J Endovasc Ther*. 2009;16:284–294.